[1] Tingting Zhang

[2] Yuhong Yang

[3] Lei Gao *

[4] Haipin He

Sustainable Urbanization-Based Data Analysis by Remote Sensing with Cyber-Physical Systems and Wireless Internet of Things Integrated Machine Learning

Abstract: - The Processing data from remote sensing has practical uses with high social worth. For example, the use of remotely sensed multispectral or radar imagery for urban monitoring, fire detection, or flood prediction can have a significant influence on both environmental and economic concerns. Remote sensing has developed into a diverse discipline that relies heavily on machine learning and signal processing techniques to handle the collected data effectively and provide accurate outputs. Some towns have been able to lessen the issue by using the various advantages provided by digitalization, which is facilitated by the internet of things and wireless connectivity. These are cyber-physical systems (CPS), which are systems in which many gadgets work together to control tangible objects. This study offers a unique method for analysing remote sensing data in metropolitan areas while modelling cyber-physical systems with wireless IoT as well as machine learning. Here, wireless IoT model in cyber-physical system has been studied using remote sensing data from metropolitan areas. Next, the environment data from the metropolitan zone was examined and categorised using regressive stochastic Gaussian modelling with Quantile adversarial neural networks (RSG-QANN). The experimental study is done in terms of precision, packet delivery ratio, end-to-end latency, recall, and accuracy of categorization. The findings demonstrate that social activity perceived signatures and physically sensed picture data, which at first glance appear to be unrelated, can in fact work in concert to improve accuracy of urban region function detection.

Keywords: urban region, remote sensing data, cyber physical system, wireless IoT, machine learning

1. Introduction:

The rate at which the global population is growing is double that of urbanisation, as evidenced by recent studies [1]. Urban convergence is a superpower that advances scientific and technical advancements as well as cross-cultural interactions. However, as wealth becomes more unequally distributed, this rapid development is creating a number of sustainability issues for resource management, urban residents' well-being, and environmental sustainability [2]. These issues include biodiversity loss, rising greenhouse gas emissions, water scarcity, and pollution. In addition, a number of systems—including those related to public morality, work, housing, transportation, and privacy—face significant obstacles and pressures, which has a detrimental impact on human existence. Urbanisation is common and often haphazard in poor nations, where the effects of urban expansion are most severe [3].As a result, it is now necessary to concentrate on urban studies and build research strategies. Regular and timely monitoring and mapping of human settlements at many spatial scales—from local to global—is vital to realising geographical and temporal diversity of population distribution and supporting global initiatives such as 2030 Agenda for Sustainable Development. Majority of this growth is anticipated to occur in emerging nations in Asia and Africa, who are presently dealing with many issues related to development, such as finding enough housing for their growing populations [4]. As a result, the global south's urbanisation causes a significant increase in urban poverty, which in turn causes impoverished and unofficial urban regions to grow (slums). This makes it abundantly evident that improved planning is required in order to achieve relevant Sustainable Development Goal (SDG), which is Sustainable Cities as well as Communities. Furthermore, swift influx of people into urban areas and the corresponding disparities have intensified the intensity and consequences of natural calamities in these regions, necessitating the implementation of efficient disaster risk mitigation tactics in line with SDG, specifically Climate Action. One of the primary elements/phases of disaster risk management is post-disaster recovery. After a disaster, recovery is typically defined as the years- or decades-long process of rebuilding as well as restoring communities to their pre-impact and normal state.Meanwhile, post-debacle recuperation brings a potential open door for the impacted region, permitting them to recognize as well as address their previous weaknesses, including disparity, better remaking of settlements, working on foundations and day to day environments in denied (ghetto) regions. This likewise addresses one of the activity needs of Sendai Structure, which is to improve debacle readiness through form

[1] Gansu Development Research Institute,Gansu Provincial Party School,Lanzhou 730050, China
[2]Zhangye Mineral Exploration Institute,Gansu Non-ferrous Metal Geological Survey Bureau,Lanzhou 730000, China
[3]College of Geology and Jewelry,Lanzhou University of resources and environment,Lanzhou 730000,China
[4]College of Geology and Jewelry,Lanzhou University of resources and environment,Lanzhou 730000,China
Email [1]esung@126.com, [2]yangyh0843@126.com, [3*]gaolei8511@126.com, [4]haipinhe@lzre.edu.cn
corresponding author: Lei Gao

back better idea in recuperation as well as reproduction method [5]. Thus, giving data in regards to the recuperation cycle, including harm evaluation after a catastrophe as well as remaking of denied/ghetto regions, is basic to help leaders and recuperation organizers to go with choices toward execution of the form back better objective successfully. Considering that the metropolitan denied regions are one of the most weak regions to fiascos, diminishing of their size during post-debacle recuperation process is a sign of fruitful form back better idea execution.One of the primary geographic information sources for assisting with the evaluation of various disaster risk management components, such as damage as well as vulnerability assessments, is remote sensing (RS) data. In order to enhance disaster risk management, several data processing and ML techniques were created to extract data from RS data. Connecting "Things" (machines and objects) to the internet and eventually to one another is the goal of the IoT, whereas CPS integrate networking, computing, and physical processes. While the IoT is somewhat more abstract as well as enables the integration of services in addition to physical things, CPS is more closely associated with machines and physical objects. CPS does not aim to provide data outside of the initial scenario; instead, it is primarily focused on specific development scenarios. IoT increases the openness of its data and services. Cyber Physical Systems, or CPSs, are what make up IoT, although they are not same as IoT devices because they are not always linked to it. CPS is a mechatronic system [6] in which things are networked to one another using information and communication technologies, either wirelessly or by wired methods. Take note that Industry 4.0, or the fourth generation of the Industrial Revolution, is a synonym for CPS. Cyber-Physical Systems use sensors to gather a great deal of environmental data. All of the dispersed knowledge in the surroundings is coupled to these sensors. A more precise action or activity may be made possible by this procedure. Cyber-Physical Systems, properly defined, are systems of computing, communication, control that are closely integrated with physical processes from several domains, including mechanical, electrical, chemical. In the realm of geoscience and remote sensing research, classification of urban visual as well as thermal hyperspectral data is a novel topic, with little research having been done thus far. The hierarchical classification technique for combining visual and thermal hyperspectral data was the main topic of the winning article in the classification area. In this case, a binary SVM classifier on concatenated feature descriptors identifies land cover classes one after the other.Furthermore, the resulting pixel-based land cover categorization map is enhanced by the use of several semantic rules, adaptive mean shift segmentation, and majority voting. The development of multiresolution as well as multisensor image analysis as well as data fusion was contributed by the paper contest winners. To enhance the spatial resolution of thermal images, visual data are used in a guided filtering method. Following the competition, the data remain openly accessible as a demanding opportunity for more image analysis research. These days, new tools like artificial intelligence (AI) as well as ML make it easier to track, comprehend, forecast growth of metropolitan regions.In order to address the intricate sustainability issues that cities face, urban analytics and modelling have grown in importance [7].

2. Related works:

In the last ten years, rapid advancements in machine learning techniques in computer vision have greatly improved land-cover-based land use categorization studies. In one study [8], for instance, a novel semitransfer deep convolutional neural network (STDCNN) method was built to handle multispectral remote sensing images with more than 3 channels as well as identify land uses at the street block level in Shenzhen and Hong Kong.Author describes a unique object-based convolutional neural network (OCBN) technique that enables more accurate and efficient categorization of urban land use from extremely fine spatial resolution remotely sensed data [9]. Notably, deep neural networks have also been used to incorporate or fuse with land cover information additional physical information about individual land parcels [10]. To train a SVM classifier, for example, [11] extracted GIST, HoG, scale-invariant feature transform-Fisher (SIFT-Fisher), other visual characteristics from street-view pictures. Residential and non-residential structures can be distinguished by the SVM classifier, which can further categorise the former into single-family and multiple homes.In work [12], land use maps at building, region, and city sizes were created by classifying roof structures using remote sensing photos and façade structures from street-view images. The author [13] evaluated the efficacy of a parcel-based land use classification technique using a RF classifier that incorporated airborne light detection and ranging (LiDAR), HRO, Google Street View (GSV) photos.Additionally, they calculated application of GSV to differentiate between other land use lots and parcels with a mix of residential and commercial buildings. Recovery assessment using RS has only recently been addressed in a few research.For example, [14] used recurrent imagery to assess Mississippi's post-Katrina reconstruction efforts. Work [15] evaluated damage as well as early recovery following an earthquake using survey and RS data. They demonstrated how RS data may offer quick assistance in assessing physical damage. But they had to manually extract the majority of the data, such building damage. In order to track post-disaster urban recovery, author [16] combined information from ground survey data with binary categorization of RS data. High-resolution remote sensing photos and ground data were used in work [17] to track the Italian recovery progress following the 2009 L'Aquila earthquake. In order to monitor structures following the Pakistani earthquake in Kashmir, work [18] developed a semi-automated object-based change detection approach employing extremely high-resolution optical pictures and

pre-disaster map data.Furthermore, throughout the post-earthquake recovery period, [19] monitored changes in land cover in urban areas using indices based on remote sensing data. They demonstrated the value of these indicators in assessing overall recovery. Each of these studies showed how crucial it is to use RS to lessen the amount of ground data needed for post-disaster recovery assessments. Recently, ML techniques are used to monitor post-disaster recovery. SVM was primary classifier employed in Work [20] to evaluate post-disaster recovery. Additionally, they developed the recovery assessment concept based on RS data as well as supplied data needed to convert changes in land cover and land use generated from RS data into positive and negative recoveries. A new automatic water extraction index (AWEI) was created by author [21] and can offer a threshold value that is quite consistent. AWEI outperformed the maximum likelihood classification (MLC) and MNDWI in the studies in terms of accuracy. Water bodies have also been delineated using colour space transformation techniques like HSV (hue, saturation, value) and HIS (hue, intensity, saturation). Work [22] separated water bodies from shadows using the HIS transformation and index composition. Work [23] introduced in-scene atmospheric adjustment to thermal hyperspectral data. Moreover, the land cover classes are identified using an SVM classifier (based on the previously described thermal feature-level fusion and visual data), and the resulting pixel-based land cover classification map is then refined using object rule-based postprocessing. A cuckoo search optimisation approach with mixed binary-continuous coding was presented by the author [24] in order to concurrently find an appropriate subset of feature representations of joint spectral-spatial dataas well as SVM hyperparameters. A hierarchical classification technique for integrating thermal spectral-textural and visual spectral-spatial feature descriptors was reported in work [25]. Using the feature descriptors listed above as a basis, a binary SVM classifier is used in this context to identify urban land cover mapping in steps.Additionally, an object rule-based postprocessing enhances resulting pixel-based land cover classification map. Road pixels are initially classified using thermal spectrum data, remaining classes are subsequently recognised by sensor fusion using the Dempster-Shafer classifier in concert with one another.

3. Contribution:

Global urbanisation is causing a rise in the difficulty of precisely mapping and monitoring these intricate landscapes. Conventional mapping techniques frequently find it difficult to keep up with the continuous changes that urban environments are experiencing. However, the strength of machine learning algorithms combined with advances in remote sensing technologies present interesting ways to get over these restrictions. At a fine geographical scale, high-resolution remote sensing data—such as photography obtained from satellites or airborne platforms—offers comprehensive information on metropolitan areas. Numerous details regarding urban elements, such as structures, roads, vegetation, and land use patterns, are captured by these data sources.Researchers may learn a great deal about urban features, spatial dynamics, and their effects on the environment by deciphering and properly interpreting this data. Use of remote sensing data to extract vegetation and built-up land is shown in this work. Visual interpretation has been utilised in previous research to delineate land use maps. We think that the traditional methods of providing geographical data are laborious and prone to human mistake. This research use machine learning in particular as a form of artificial intelligence.

4. Proposed wireless IoT model in cyber physical system for urban region remote sensing data:

A wireless control system is made up of wireless mesh networked feedback control loops that link sensors, controllers, and actuators. Plant variables are measured by sensors, which transmit the data to a controller via a wireless mesh network. The physical processes are then controlled by the actuators receiving control orders from the controller. Industry plants have challenging wireless communication settings because of physical barriers, coexisting wireless devices, multipath fading, and high channel noise. The network manager is in charge of organising, planning, setting up the routes, and managing the network.As seen in Fig. 1, network devices consist of a gateway, numerous access points, and a collection of field devices. The Gateway is where the controllers and network management are placed or linked. The wireless sensors and actuators are the field devices. Every field device has an IEEE 802.15.4-compliant half-duplex omnidirectional radio transceiver installed. To offer redundant pathways between the wireless network and the Gateway, several access points are linked to it.

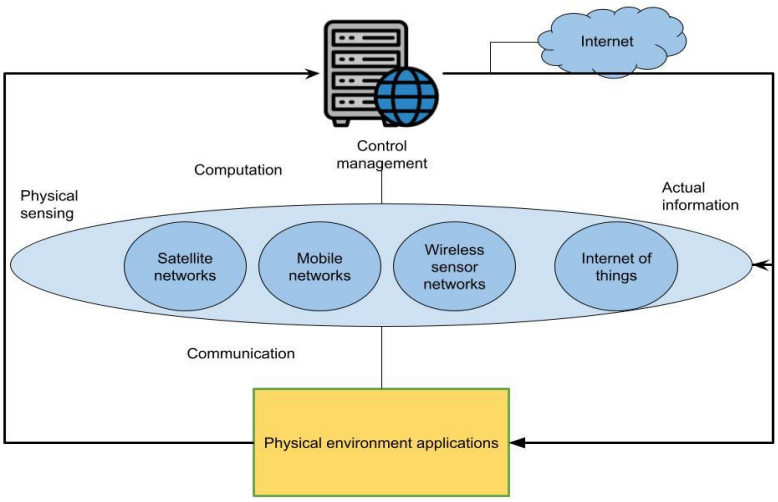

Figure-1 wireless IoT based CPS architecture

For CPSN systems, precise output decision prediction and sensing information dependability are deemed essential. As a result, it is imperative to precisely specify the network demand parameters for both the physical and cyber domains (Figure 2). QoS foundation for developing a real-time intelligent system for high-stress and limited situations, such as mining, healthcare, and warfare, is likewise formed by these elements. For cyber systems, quality of service (QoS) elements like prompt delivery to the monitoring station and smooth data flows over the cloud are deemed essential. When CPS is combined with additional methods, such as semantic agents as well as cloud-based hybrid system states, situation gets more complicated.Positioning of sensor as well as actuator devices at strategically important locations, together with clever methods for node localization as well as geolocation recognition, are necessary for the deployment of CPSN architectural components. When negotiating between nearby data collecting devices and sensors, Medium Access Control (MAC) on sensing side should take into account need to save resources like as bandwidth, number of channels, buffer storage, transmission energy.

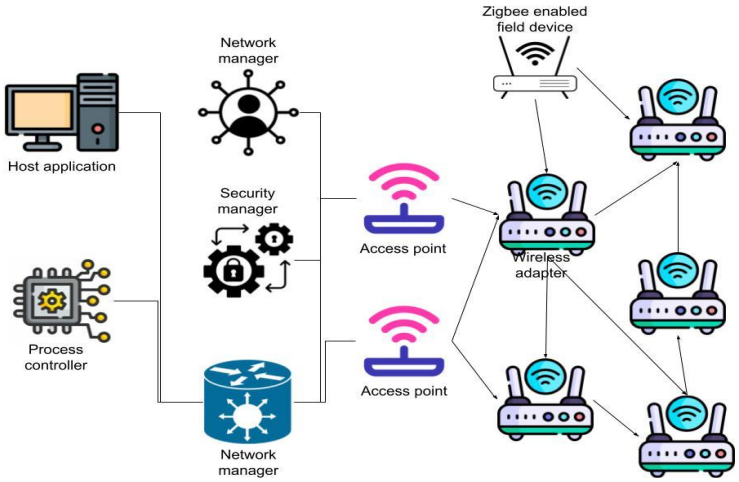

Figure-2 wireless sensor network setup with central monitoring

Here, virtual sensors Sc, virtual actuators Ac, functional units Fc, observed events Ec, virtual interfaces Nc, virtual power supply Pc, and data storage Dc make up c = (Sc, Ac, Fc, Ec,Nc, Pc, Dc). Here, the virtual power supply denotes that cloud-based process may be simply installed or deleted from cloud, virtual interface is the digital twin's communication medium that is connected to the actual object. The observable outputs of a physical item are the virtual sensors of a cyber entity, often known as a digital twin. These observations can be either the events themselves or raw data that will be processed by a cyber thing's cloud-based functional units to detect happenings. The link between a cyber object and a physical thing is represented by equation 6.A physical object can always function on its own without the assistance of a cyber object. On the other hand, it is not feasible to replace a physical object entirely with a cyber one (1−1 c 6= 1c).A cyber object expands a physical object's capabilities. Thus, in a C2PS, there need to be a minimum of one cyber entity for every physical entity, $|C| \geq |P|$. Finite state machine in sequence Equations 1 apply to the cyber objects in the same way.

$$C = \{cj, j = 1 \ldots\ldots |c|\} \quad (1)$$

In general, any spatial database has three types of data: spatial vectors, attribute features, metadata. Additionally, there are three different kinds of spatial data: (1) spatial vector data, which are typically points, lines, polygons; (2) raster data, which is also referred to as data grids; (3) picture data, which include data from remote sensing, which is a more sophisticated concept. The size of attribute data, which are indexed data, typically consists of n items arranged in rows and j attributes listed in columns. The columns contain the attributes of entities, and each row represents an item. This traditional form of data might originate from surveys as well as various sources based on sensors.Because attribute data have better model correctness, they are simpler to analyse using statistical techniques or basic learning algorithms. They do, however, have the drawback of being costly or difficult to procure over a wide geographic area. As a result, they make it possible to perform tasks on a small size with increased precision and accuracy because these kinds of data sets are frequently combined to provide information on a larger scale.Apart from the aforementioned two types of data, metadata are the most often overlooked data type, despite their frequent usage, particularly in cases where another user will subsequently access the database. They provide details regarding the data's generation, projection, accuracy, scale, and/or datum as well as their acquisition, collection, and processing methods.

Regressive stochastic Gaussian modelling with Quantile adversarial neural networks in environment data analysis:

It is comparable to ridge regression, but with minor but significant variations. The definition of the lasso estimate is as follows by eqn (2)

$$\hat{\beta}^{\text{Lasso}} = \min_{\beta} \sum_{i=1}^{N} \left(y_i - \beta_0 - \sum_{j=1}^{p} x_{ij}\beta_j \right)^2 \quad \text{s.t. } \sum_{j=1}^{p} |\beta_j| \leqslant t \quad (2)$$

where restriction on total absolute value of all coefficients β is t > 0. After data are standardised, $\bar{y}$, or the mean value of y, is the solution for β0, and a model without an intercept can then be fitted. The Lasso problem has an equivalent Lagrangian form that is by eqn (3)

$$\hat{\beta}^{\text{Lasso}} = \min_{\beta} \sum_{i=1}^{N} \left(y_i - \beta_0 - \sum_{j=1}^{p} x_{ij}\beta_j \right)^2 \quad (3)$$

Alternatively, the lasso signal approximator (LSA) is expressed as eqn (4)

$$\min_{x} \frac{1}{2} \| x - y \|_2^2 + \lambda_1 \| x \|_1 + \lambda_2 \| Dx \|_1 \quad (4)$$

where $\|.\|_1$ is l_1 norm, and $D \in R^{(n-1)\times n}$ is defined as eqn (5)

$$D = \begin{bmatrix} 1 & -1 & 0 & \ldots 0 & 0 \\ 0 & 1 & -1 & \ldots 0 & 0 \\ \vdots & \vdots & \ddots & \vdots & \vdots \\ 0 & 0 & \ldots & 1 & -1 \end{bmatrix} \quad (5)$$

Since x_i is only one if $x_i > 0$ and −1 otherwise, the derivative of $\| x \|_1$ is not defined at zero. As a result, one may write by eqn (6)

$$w_i = \begin{cases} \lambda_1 & \text{if } x_i > 0 \\ \in [-\lambda_1, \lambda_1] & \text{if } x_i = 0 \\ -\lambda_1 & \text{if } x_i < 0 \end{cases} \quad (6)$$

The popular projection operator is utilized to restate requirements in (7) as

$$w = P_{\lambda_1}(w + x),$$

where $P_{\lambda_1}(a) = \left[P_{\lambda_1}(a_1), P_{\lambda_1}(a_2), \ldots, P_{\lambda_1}(a_n)\right]$, and

$$P_{\lambda_1}(a_i) = \begin{cases} \lambda_1 & \text{if } a_i > \lambda_1 \\ \in [-\lambda_1, \lambda_1] & \text{if } |a_i| \leq \lambda_1 \\ -\lambda_1 & \text{if } a_i < -\lambda_1. \end{cases} \quad (7)$$

$$\mathrm{p}(x) = \sum_{j=1}^{K} \pi_j p(x; \theta_j), \; j = 1, \ldots, K.$$

$$p(\mathbf{x}) = \sum_{c=1}^{C} \pi_c f_c(\mathbf{x} \mid \theta) \quad (8)$$

Mixture method has a vector of parameters, $\underline{\theta} = \{\theta_1, \ldots, \theta_k, \pi_1, \ldots \pi_k\}$

$$p(z, x) = p(z)p(x \mid z)$$

$$p(z_k = 1) = \pi_k \quad (9)$$

PDF of X is described by equation (10).

$$p(x \mid \mu_k, \Sigma_k) = \frac{1}{\sqrt{2\pi|\Sigma^{-1}|}} \exp\left(-\frac{1}{2}(x - \mu_x)\Sigma_x^{-1}(x - \mu_x)^T\right)$$

$$f_c(\mathbf{x} \mid \boldsymbol{\mu}_c, \boldsymbol{\Sigma}_c) = \frac{1}{(2\pi)^{\frac{d}{2}}|\boldsymbol{\Sigma}_c|^{\frac{1}{2}}} \exp\left(-\frac{1}{2}(\mathbf{x} - \boldsymbol{\mu}_c)^t \boldsymbol{\Sigma}_c^{-1}(\mathbf{x} - \boldsymbol{\mu}_c)\right) \quad (10)$$

Equation (11) represents a Gaussian mixed distribution using a linear superposition of Gaussians.

$$p(x) = \sum_{k=1}^{K} \pi_k p(x \mid \mu_k, \Sigma_k)$$
$$\hat{\pi}_c = \frac{n_c}{n},$$
$$\hat{\mu}_c = \frac{1}{n_c} \sum_{\{f \mid y_i = c\}} \mathbf{x}_i$$
$$\hat{\mathbf{\Sigma}}_c = \frac{1}{(n_c - 1)} \sum_{\{i \mid y, = c\}} (\mathbf{x}_i - \boldsymbol{\mu}_c)(\mathbf{x}_i - \boldsymbol{\mu}_c)^t \quad (11)$$

Given a specific value of z, conditional distribution of x is now a Gaussian by eqn (12):

$$p(x \mid z_k = 1) = p(x \mid \mu_k, \Sigma_k)$$
$$p(x \mid z) = \prod_{k=1}^{K} p(x \mid \mu_k, \Sigma_k)^{z_k} \quad (12)$$

Equation (13) can be used to derive marginal distribution of x by summing joint distribution of all possible states of z.

$$p(x) = \sum_z p(z) p(x \mid z) = \sum_{k=1}^{K} \pi_k p(x \mid \mu_k, \Sigma_k) \quad (13)$$

A significant derived quantity eqn(14) is "posterior probability" on a mixture component for a given data vector:

$$\gamma(z_k) \equiv p(z_k = 1 \mid x) = \frac{p(z_k=1) p(x \mid z_k=1)}{\sum_{j=1}^{K} p(z_j=1) p(x \mid z_j=1)} = \frac{\pi_k p(x \mid \mu_k, \Sigma_k)}{\sum_{j=1}^{K} \pi_j p(x \mid \mu_j, \Sigma_j)} \quad (14)$$

Examine the following examples for a binary classification problem: z = (x, y) ∈ R d −1,+1}. The fundamental cost function is reduced in order to produce linear Q-learning classifier by eqn (15)

$$P_n(\mathbf{w}) = \frac{\lambda}{2} \parallel \mathbf{w} \parallel^2 + \frac{1}{n} \sum_{i=1}^{n} \ell(y_i \mathbf{w}^\top \mathbf{x}_i) = \frac{1}{n} \sum_{i=1}^{n} \left(\frac{\lambda}{2} \parallel \mathbf{w} \parallel^2 + \ell(y_i \mathbf{w}^\top \mathbf{x}_i) \right) \quad (15)$$

$$\bar{U} = \left\{ \mathbf{u} \in \mathbb{R}^n \text{ such that } \mathbf{u} = \sum_{j=1}^{m} \alpha_j \mathbf{u}_j; \alpha_j \in \mathbb{R}^+ (\forall j); \sum_{j=1}^{m} \alpha_j = 1 \right\} \quad (16)$$

The corresponding scalar product of a n × n real-symmetric positive-definite matrix by eqn (17)

$$(\mathbf{u}, \mathbf{v}) = \mathbf{u}^t \mathbf{A}_n \mathbf{v} (\mathbf{u}, \mathbf{v} \in \mathbb{R}^n)$$
$$\parallel \mathbf{u} \parallel = \sqrt{\mathbf{u}^t \mathbf{A}_n \mathbf{u}} \quad (17)$$

The goal of reinforcement learning (RL) is to select the best course of action over time in order to maximise the expected value of the return by eqn (18)

$$G_t = R_{t+1} + \gamma R_{t+2} + \cdots = \sum_{k=0}^{\infty} \gamma^k R_{t+k+1} \quad (18)$$

When policy π is followed, long-term value of state s is provided by state-value function vπ(s). State-value function is divided into two components: discounted value of successor state γvπ(St+1) as well as immediate reward Rt+1.

The function of action-value The expected return is qπ(s, a), where s is initial state, an is action, and π is policy by eqn (19)

$$q_\pi(s, a) = \mathbb{E}_n[G_t \mid S_t = s, A_t = a] \quad (19)$$

Our definition of Ra s = E[Rt+1|St = s, At = a] simplifies notations. Link between vπ(s) and qπ(s, a) is also discernible by eqn (20)

$$v_\pi(s) = \sum_{a \in \mathcal{A}} \pi(a \mid s) q_\pi(s, a)$$
$$q_*(s, a) = \mathcal{R}_s^a + \gamma \sum_{s' \in \mathcal{S}} \mathcal{P}_{ss'}^a v_\pi(s')$$
$$v_\pi(s) = \sum_{a \in \mathcal{A}} \pi(a \mid s) \left(\mathcal{R}_s^a + \gamma \sum_{s' \in \mathcal{S}} \mathcal{P}_{ss'}^a v_\pi(s') \right) \quad (20)$$

State-value function of one state and that of other states are related by Bellman equation. Bellman eqn for qπ(s, a),$q * (s, a) = \mathcal{R}_s^a + \gamma \sum_{s' \in \mathcal{S}} \mathcal{P}_{ss'}^a \max_{a'} q_*(s', a')$.

Using the theorem, we can quickly determine the best course of action by maximising q∗(s, a) across all actions by eqn (21)

$$\pi_*(a \mid s) = \begin{cases} 1 & \text{if } a = \arg\max_{a \in \mathcal{A}} q_*(s, a), \\ 0 & \text{otherwise.} \end{cases}$$
$$v_*(s) = \max_a q_*(s, a),$$
$$q_*(s, a) = \mathcal{R}_s^a + \gamma \sum_{s' \in \mathcal{S}} \mathcal{P}_{ss'}^a v_*(s')$$
$$v_*(s) = \max_a \left(\mathcal{R}_s^a + \gamma \sum_{s' \in \mathcal{S}} \mathcal{P}_{ss'}^a v_*(s') \right) \quad (21)$$

We also have a Bellman equation for q∗.

$$q * (s, a) = \mathcal{R}_s^a + \gamma \sum_{s' \in \mathcal{S}} \mathcal{P}_{ss'}^a \max_{a'} q_*(s', a'). \quad (22)$$

Batch-wise training variations originate from gradient variance. Noisy gradient is a drawback of employing a random sample to approximate population; it requires far less computations each cycle. Note that this section uses iterations to measure convergence rate. We must first define Lyapunov process to examine training dynamics for each iteration by eqn (23)

$$h_t = \|\mathbf{w}' - \mathbf{w}^*\|_2^2 \quad (23)$$

Additionally, because it can improve the input data's feature representation quality, model depth is important for classification performance. Higher model depths primarily take advantage of more abstract and invariant aspects of the original data. In this regard, several comparative experiments are conducted to calculate extent to which the classification performance is defined by the depth parameter.

5. Experimental results:

The suggested architecture with fog and cloud nodes is evaluated on a server with a Core E7400 CPU, 3.00 GB of RAM, and a 32-bit operating system working at 2.80 GHz.

Dataset description:A number of such datasets remain private, primarily due to security concerns, although some are now available to the public, including DARPA 98, KDD99, and UNSW-NB15. Not many actual IoT as well as network traffic datasets that include new Botnet instances have been developed, despite the fact that many datasets have been created. Furthermore, several databases lack IoT-generated traffic, while others don't incorporate any fresh functionalities.

Table-1 Comparative based on various malicious attack datasets

Dataset	Techniques	Classification accuracy	Recall	End-End delay	PDR	Precision
DARPA 98	**SVM**	89	59	45	81	82
	SYN-DOS	92	62	44	83	85
	RSG-QANN	93	63	42	85	88
KDD99	**SVM**	92	65	48	82	89
	SYN-DOS	94	68	46	84	92
	RSG-QANN	96	72	44	86	93
UNSW-NB15	**SVM**	95	58	52	85	85
	SYN-DOS	96	72	50	88	88
	RSG-QANN	98	74	45	92	92

Based on several harmful attack datasets, the comparison study between suggested and current techniques is displayed in table 1 above. The datasets studied in this case are UNSW-NB15, KDD99, and DARPA 98. In terms of categorization accuracy, recall, PDR, end-end delay, and precision, parametric analysis is conducted.

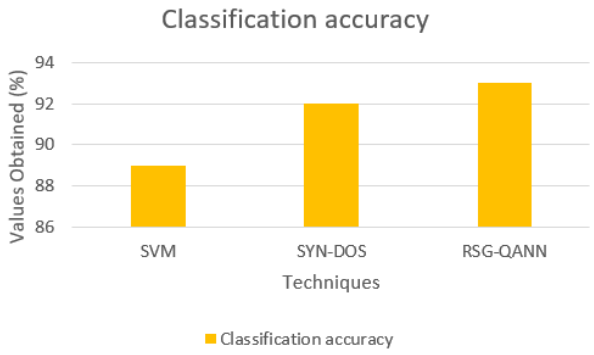

(a) classification accuracy

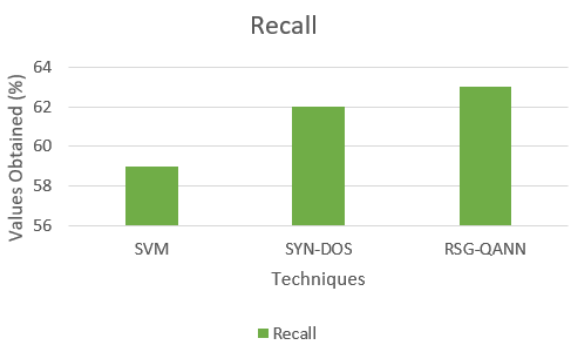

(b) recall

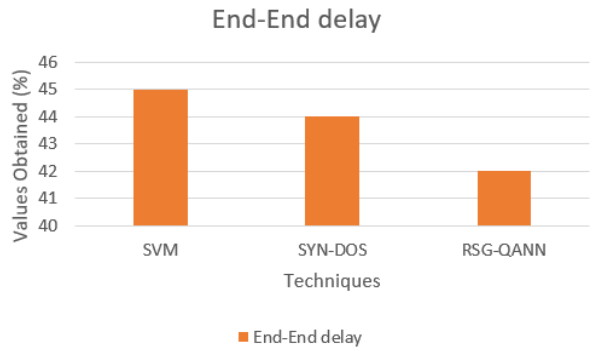

(c) end-end delay

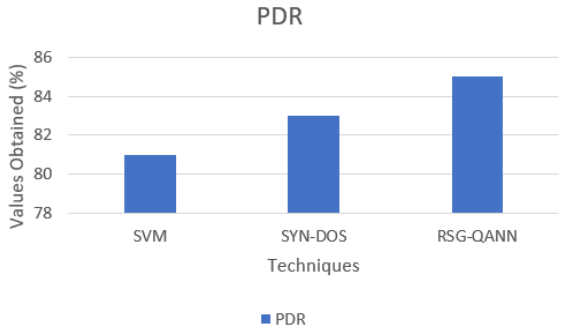

(d) packet delivery ratio

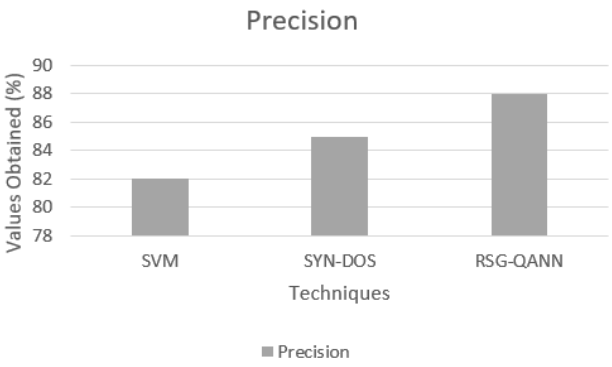

(e) precision

Figure-3 Comparative for DARPA 98 dataset

Figures 3(a) through (e) above compare suggested and current methods for the DARPA 98 dataset. While the existing SVM achieved classification accuracy of 89%, recall of 59%, end-end delay 45%, PDR of 81%, precision 82%, SYN-DOS achieved classification accuracy 92%, recall 62%, end-end delay of 44%, PDR 83%, precision 88%, proposed technique achieved these same results.

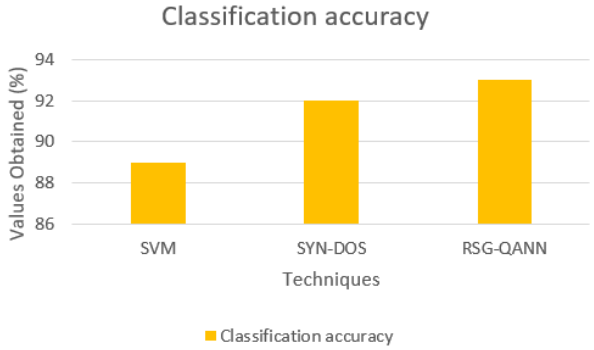

(a) classification accuracy

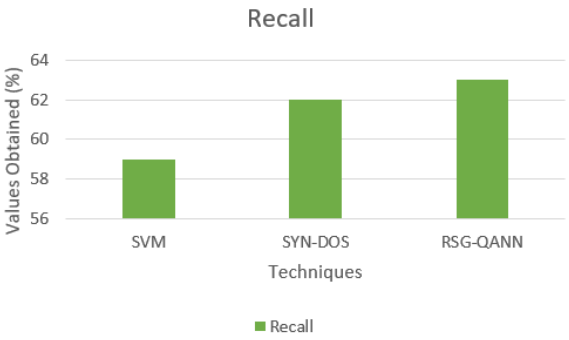

(b) recall

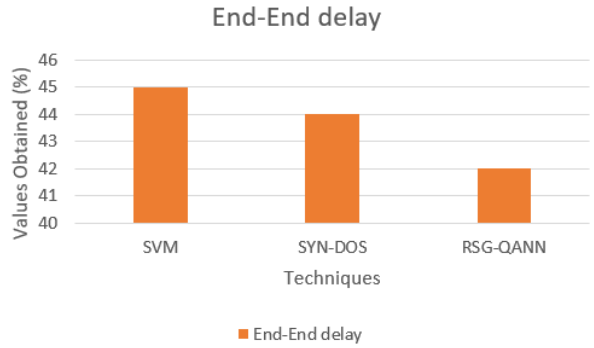

(c) end-end delay

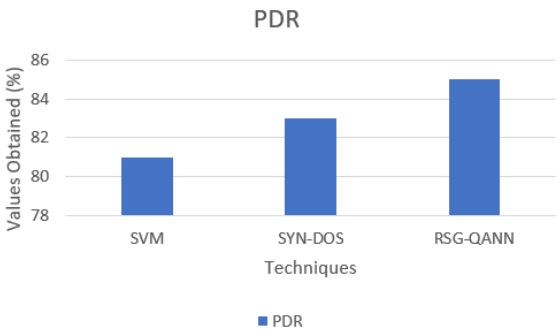

(d) packet delivery ratio

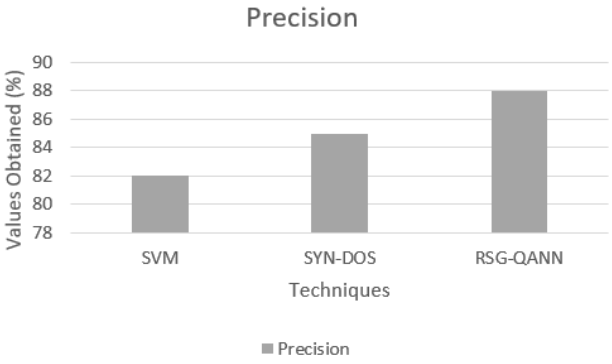

(e) precision

Figure-4 Comparative for KDD99dataset

The KDD99 dataset-based comparison analysis of suggested and current approaches is displayed in figures 4(a) through (e) above. In this case, the suggested method achieved 96% classification accuracy, 72% recall, 44% end-end delay, 86% PDR, 93% precision; the current SVM achieved 92% classification accuracy, 65% recall, 48% end-end delay, 82% PDR, 89% precision; SYN-DOS achieved 94% classification accuracy, 68% recall, 46% end-end delay, 84% PDR, 92% precision.

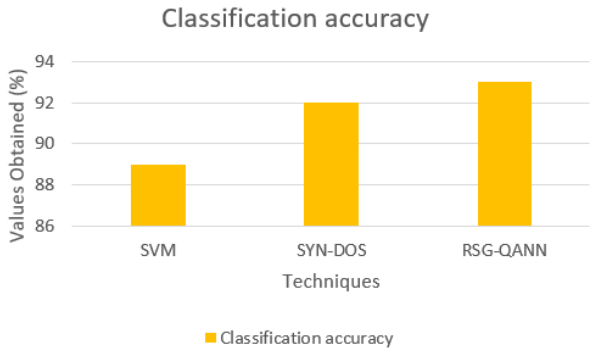

(a) classification accuracy

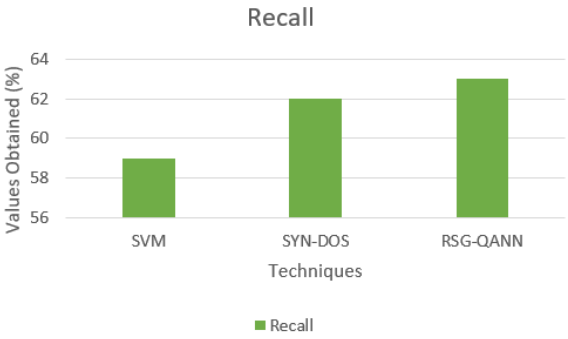

(b) recall

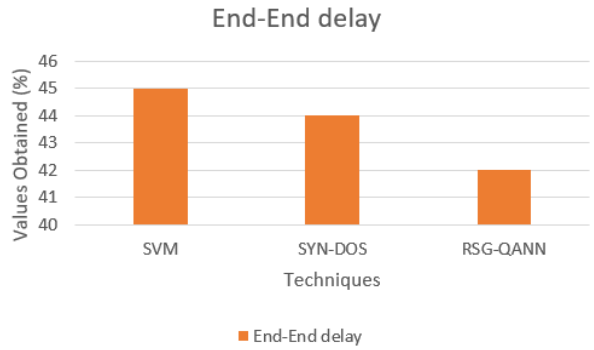

(c) end-end delay

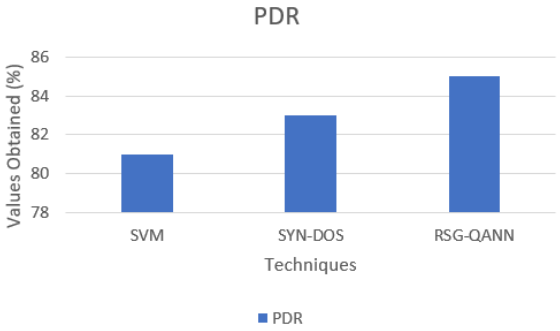

(d) packet delivery ratio

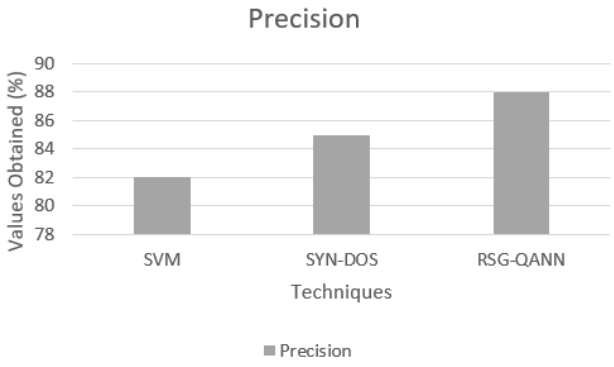

(e) precision

Figure-5 Comparative for UNSW-NB15 dataset

For the UNSW-NB15 dataset, the comparison analysis between suggested and current methodologies is displayed in Figure 5(a)–(e) above. The suggested method achieved 98% classification accuracy, 74% recall, 45% end-end delay, 92% PDR, 92% precision; the current SVM method achieved 95% classification accuracy, 58% recall, 52% end-end delay, 85% PDR, 85% precision; SYN-DOS method achieved 96% classification accuracy, 72% recall, 50% end-end delay, 88% PDR, 88% precision.

From 2013 to 2015 and from 2017 to 2019, the area of urban areas decreased by 14.14 km2 and 0.79 km2, respectively. From 2015 to 2017 and 2019 to 2021, the area of urban areas increased by 15.17 and 2.38 km2, respectively. Vegetated land is 60-70 km2 , besides in 2015, which expanded to 82.40 km2 . Except for 2019, when it was reduced to 0.00 km2, the water area was between 1.7 and 3 km2. This warming of ocean surface reduces precipitation in Indonesian district and increases the focal Pacific Sea's capacity for cloud formation.Conditions for the dry season are triggered throughout the entire Indonesian domain by the El Niño anomaly. When La Niña occurs, the central Pacific Sea's ocean surface temperatures drop below average. The focal Pacific Sea's ability to form clouds is reduced by this dropping of the ocean surface temperature, which

also increases precipitation overall in Indonesia.Because the research site is on Bali Island's southern coast, it has a lot to do with the effects of climate change and coastal dynamics. Recognizing the functions of the urban region is essential to rational urban planning as well as management. It refers to inference of purposes for which urban areas are used, including residential, commercial, entertainment, and educational purposes, that are directly associated with human activities. It is related to but also distinct from the conventional classification of LULC.Former focuses solely on socioeconomic and functional characteristics of urban regions, while the latter typically emphasizes physical characteristics of earth's surface. LULC observing utilizing remote detecting symbolism is demonstrated to be proficient as well as successful, since these pictures can well catch the normal appearance of land surface. In any case, district capability acknowledgment utilizing remote detecting pictures alone isn't adequate, particularly in high-thickness urban areas, like Shenzhen, London, and New York. This is because of following information: 1) Urban region functions are influenced by related human activities and have socioeconomic properties; (2) shadows of various elevated structures in high-thickness urban areas present extraordinary difficulties for remote detecting picture handling; (3) blended metropolitan capabilities are in many cases grouped in one structure or block in east Asian urban communities.

6. Conclusion:

This research propose novel technique in urban region based data analysis for CPS in remote wireless IoT model using machine learning in regressive stochastic Gaussian modelling with Quantile adversarial neural networks (RSG-QANN) for environmental data analysis. Measured accuracy values for classification findings show how resilient recommended strategy is in extracting slum zones in a challenging environment, even in an event time image with debris as well as rubble land coverings. Next, we created related maps of damage and recovery, which displayed the slums that were damaged, recovered, not recovered from, and freshly constructed. We then spoke about these maps from the perspectives of vulnerability assessment and better building. The created techniques may be applied in any other place or during any kind of crisis to monitor and assess urban poor communities. The machine learning techniques' parameters need to be adjusted for the particular case study in order to extract impoverished regions from multi-temporal remote sensing photos.But adding other forms of data, including survey data, can help create a more thorough assessment of societal risk and, consequently, better construct back stronger idea assessments. A series of tests was conducted to analyse the execution time as well as impact of method depth on aforementioned dataset. To obtain better classification accuracy and minimise execution time, we recommend using a deep learning model. In further research, we will examine the use of pre-trained networks to reduce the enormous amount of labour needed to retrain the deep learning architecture.

Reference:

[1] Youssef, R., Aniss, M., & Jamal, C. (2020, March). Machine learning and deep learning in remote sensing and urban application: A systematic review and meta-analysis. In *Proceedings of the 4th Edition of International Conference on Geo-IT and Water Resources 2020, Geo-IT and Water Resources 2020* (pp. 1-5).

[2] Mostafa, E., Li, X., Sadek, M., & Dossou, J. F. (2021). Monitoring and forecasting of urban expansion using machine learning-based techniques and remotely sensed data: A case study of gharbia governorate, Egypt. *Remote Sensing*, *13*(22), 4498.

[3] Xu, M., Sun, C., Zhan, Y., & Liu, Y. (2023). Impact and prediction of pollutant on mangrove and carbon stocks: A machine learning study based on urban remote sensing data. *Geoscience Frontiers*, 101665.

[4] Cao, R., Tu, W., Yang, C., Li, Q., Liu, J., Zhu, J., ... & Qiu, G. (2020). Deep learning-based remote and social sensing data fusion for urban region function recognition. *ISPRS Journal of Photogrammetry and Remote Sensing*, *163*, 82-97.

[5] de Arruda Moreira, G., Sánchez-Hernández, G., Guerrero-Rascado, J. L., Cazorla, A., & Alados-Arboledas, L. (2022). Estimating the urban atmospheric boundary layer height from remote sensing applying machine learning techniques. *Atmospheric Research*, *266*, 105962.

[6] Rao, P., Tassinari, P., & Torreggiani, D. (2023). Exploring the land-use urban heat island nexus under climate change conditions using machine learning approach: A spatio-temporal analysis of remotely sensed data. *Heliyon*, *9*(8).

[7] Lyu, F., Wang, S., Han, S. Y., Catlett, C., & Wang, S. (2022). An integrated cyberGIS and machine learning framework for fine-scale prediction of Urban Heat Island using satellite remote sensing and urban sensor network data. *Urban Informatics*, *1*(1), 6.

[8] Li, F., Yigitcanlar, T., Nepal, M., Nguyen, K., & Dur, F. (2023). Machine Learning and Remote Sensing Integration for Leveraging Urban Sustainability: A Review and Framework. *Sustainable Cities and Society*, 104653.

[9] Chen, P., Wang, B., Wu, Y., Wang, Q., Huang, Z., & Wang, C. (2023). Urban river water quality monitoring based on self-optimizing machine learning method using multi-source remote sensing data. *Ecological Indicators*, *146*, 109750.

[10] Ghaffarian, S., & Emtehani, S. (2021). Monitoring urban deprived areas with remote sensing and machine learning in case of disaster recovery. *Climate*, *9*(4), 58.

[11] Alwan, A. A., Ciupala, M. A., Brimicombe, A. J., Ghorashi, S. A., Baravalle, A., & Falcarin, P. (2022). Data quality challenges in large-scale cyber-physical systems: A systematic review. *Information Systems*, *105*, 101951.

[12] Brighente, A., Conti, M., Di Renzone, G., Peruzzi, G., & Pozzebon, A. (2023). Security and Privacy of Smart Waste Management Systems: A Cyber-Physical System Perspective. *IEEE Internet of Things Journal*.

[13] Rani, S., Kataria, A., Chauhan, M., Rattan, P., Kumar, R., & Sivaraman, A. K. (2022). Security and privacy challenges in the deployment of cyber-physical systems in smart city applications: State-of-art work. *Materials Today: Proceedings*, *62*, 4671-4676.
[14] Chae, J., Lee, S., Jang, J., Hong, S., & Park, K. J. (2023). A Survey and Perspective on Industrial Cyber-Physical Systems (ICPS): From ICPS to AI-Augmented ICPS. *IEEE Transactions on Industrial Cyber-Physical Systems*.
[15] Singh, A. K., Pamula, R., & Srivastava, G. (2022). An adaptive energy aware DTN-based communication layer for cyber-physical systems. *Sustainable Computing: Informatics and Systems*, *35*, 100657.
[16] Salau, B. A., Rawal, A., & Rawat, D. B. (2022). Recent advances in artificial intelligence for wireless internet of things and cyber–physical systems: A comprehensive survey. *IEEE Internet of Things Journal*, *9*(15), 12916-12930.
[17] Hamdan, S., Almajali, S., Ayyash, M., Salameh, H. B., & Jararweh, Y. (2023). An intelligent edge-enabled distributed multi-task learning architecture for large-scale IoT-based cyber–physical systems. *Simulation Modelling Practice and Theory*, *122*, 102685.
[18] Faheem, M., & Butt, R. A. (2022). Big datasets of optical-wireless cyber-physical systems for optimizing manufacturing services in the internet of things-enabled industry 4.0. *Data in Brief*, *42*, 108026.
[19] Alzahrani, A., Alshehri, M., AlGhamdi, R., & Sharma, S. K. (2023, January). Improved Wireless Medical Cyber-Physical System (IWMCPS) Based on Machine Learning. In *Healthcare* (Vol. 11, No. 3, p. 384). MDPI.
[20] Rajawat, A. S., Bedi, P., Goyal, S. B., Shaw, R. N., & Ghosh, A. (2022). Reliability analysis in cyber-physical system using deep learning for smart cities industrial IoT network node. *AI and IoT for Smart City Applications*, 157-169.
[21] Huang, Z., Qi, H., Kang, C., Su, Y., & Liu, Y. (2020). An ensemble learning approach for urban land use mapping based on remote sensing imagery and social sensing data. *Remote Sensing*, *12*(19), 3254.
[22] Wurm, M., Droin, A., Stark, T., Geiß, C., Sulzer, W., & Taubenböck, H. (2021). Deep learning-based generation of building stock data from remote sensing for urban heat demand modeling. *ISPRS International Journal of Geo-Information*, *10*(1), 23.
[23] Hartling, S., Sagan, V., & Maimaitijiang, M. (2021). Urban tree species classification using UAV-based multi-sensor data fusion and machine learning. *GIScience & Remote Sensing*, *58*(8), 1250-1275.
[24] Yagoub, M. M., Tesfaldet, Y. T., Elmubarak, M. G., & Al Hosani, N. (2022). Extraction of Urban Quality of Life Indicators Using Remote Sensing and Machine Learning: The Case of Al Ain City, United Arab Emirates (UAE). *ISPRS International Journal of Geo-Information*, *11*(9), 458.
[25] Tian, S., Zhong, Y., Zheng, Z., Ma, A., Tan, X., & Zhang, L. (2022). Large-scale deep learning based binary and semantic change detection in ultra high resolution remote sensing imagery: From benchmark datasets to urban application. *ISPRS Journal of Photogrammetry and Remote Sensing*, *193*, 164-186.